ISBN: 978-3-95450-211-0 doi:10.18429/JACoW-SRF2019-THP097

FIELD EMISSION STUDIES ON ESS ELLIPTICAL PROTOTYPE CAVITIES AT CEA SACLAY

Enrico Cenni†, Matthieu Baudrier, Guillaume Devanz, Luc Maurice, Olivier Piquet, Dominique Roudier, CEA Université Paris-Saclay, Gif-sur-Yvette, France.

Abstract

For the development of efficient superconducting cavities, field emission is an important parasitic phenomena to monitor. A diagnostic system composed of Geiger-Mueller (G-M) probes, NaI(Tl) scintillators and PIN diodes has been installed on vertical and cryomodule test stand. Collected data is analysed and confronted to particle tracking simulation. Such systematic analysis allows the identification of the most probable location origin of the field emission.

INTRODUCTION

CEA Saclay is in charge of the superconducting elliptical cavity prototypes for the European Spallation Source (ESS). This involves the design, the manufacturing, the testing and the integration of the cavity into demonstrator cryomodules. A set of 6 medium beta and 5 high beta cavities have been manufactured. As part of these activities, we are interested in field emission issue as one of the limiting factors for cavity performances. Data on cavities operated in vertical cryostat and inside cryomodules are currently being collected, analysed by means of particle tracking simulation and compared to radiation dose monitoring and scintillators. Herein, our latest results on vertical tests and medium beta cryomodule demonstrator tests (MECCTD) are reported.

DESCRIPTION OF THE CAVITIES

In this section, some relevant RF parameters and requirements for medium and high beta elliptical cavity section will be presented. More details are available elsewhere [1-3]. Two types of elliptical cavities were developed in CEA-Saclay. One called medium beta has a geometrical beta of 0.67 while the second has a geometrical beta of 0.86 and is called high beta. Some relevant parameters concerning cavity design and expected performance are listed in Table 1.

The two cavity models integrated with the helium tank are shown in Fig. 1. A mid-section view is used to appreciate the inner geometry

The two most relevant quantities concerning field emission are the ratio E_{pk}/E_{acc} and the accelerating field required during operation. This is due to the strong dependence of field emission current and surface electric field as demonstrated by Fowler and Nordheim [4] with equation (1).

$$J = \frac{A(\beta E_{surf})^2}{\varphi} e^{-\frac{B\varphi^{1.5}}{\beta E_{surf}}} \quad [\frac{A}{m^2}] \qquad (1)$$

Table 1: Design Parameters and Performance Requirements

Design parameters	Medium beta	High beta
Geometrical beta - β_{geom}	0.67	0.86
Nominal gradient E_{acc} [MV/m]	16.7	19.9
Q_0 at nominal gradient	$> 5 \times 10^9$	
E_{pk}/E_{acc}	2.36	2.2
B_{pk}/E_{acc} [mT/(MV/m)]	4.79	4.3
E_{pk}@nominal E_{acc} [MV/m]	39	44
B_{pk}@nominal E_{acc} [mT]	80	85

Where A and B are constant, φ is the material work function, E_{surf} is the electric field on the surface and β is the geometrical enhancing factor due to surface asperity.

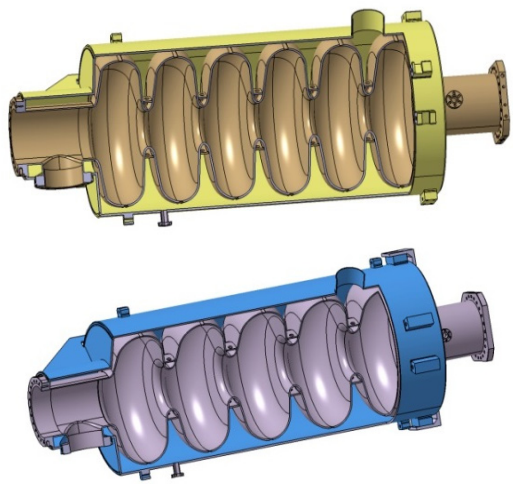

Figure 1: High beta (top) and medium beta (bottom) mid cross section.

X-RAY DIAGNOSTIC SYSTEM

CEA Saclay is in charge of the assembly of all ESS elliptical cavities cryomodule and to assess the performance of two prototypes MECCTD, the high beta cryomodule demonstrator (HECCTD) and six from series (three from each model). In the last years we are steadily increasing the diagnostic during our tests in the vertical cryostat and more recently in the cryomodule test stand. Three types of devices are used: Geiger-Mueller (G-M) probes, NaI(Tl) scintillators and PIN diodes.

Vertical Cryostat

In the vertical cryostat, data are collected during cavity test through the three types of devices: a G-M probe and

ISBN: 978-3-95450-211-0 doi:10.18429/JACoW-SRF2019-THP097

NaI(Tl) scintillators are installed on the test stand top plate and a set of PIN diodes cover the cavity beam pipes, as shown in Figs. 2 and 3. Two sets of 16 PIN diodes were installed on the beam pipe flange at the cavity ends. The model and acquisition electronics can be found elsewhere [5–7].

Figure 2: High beta cavity installed in vertical test stand.

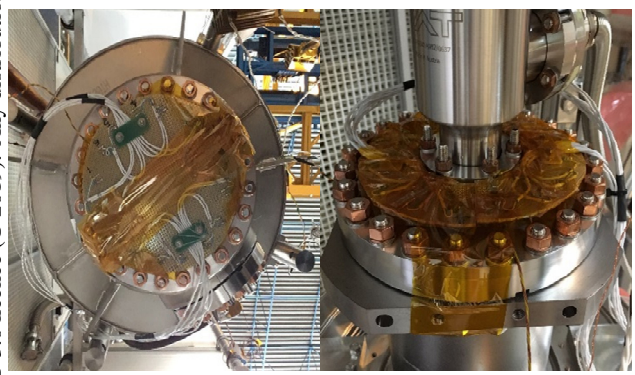

Figure 3: PIN diodes installed on the beam pipe flange coupler side (left) and tuner side (right).

Cryomodule

In the cryomodule, data are collected via a G-M probe and NaI(Tl) scintillators.

The limited number of detectors, whose location can be seen in Fig. 4, were used during the first cryomodule test. A NaI(Tl) scintillator was located just below the beam axis on one side of the cryomodule (red square in Fig. 4) and one G-M detector was positioned below the powered cavity at the beginning of each test (only one cavity was operated at the time).

Figure 5 presents the scintillator set up: a lead shielding was built around it in order to limit pile up events during operation and a 3mm aperture (top right corner in Fig. 5) was used as collimator.

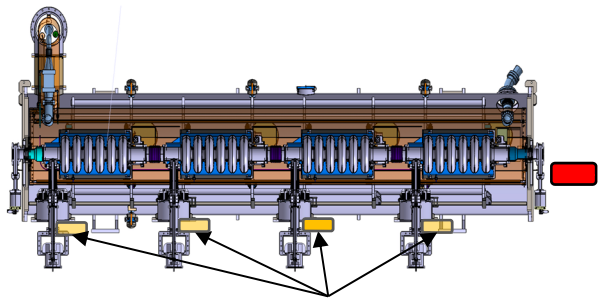

Figure 4: Medium beta cryomodule prototype (MECCTD) cavity are numbered from right to left (CAV1-CAV4), NaI(Tl) scintillator (red box) and a dose rate G-M detector (yellow box).

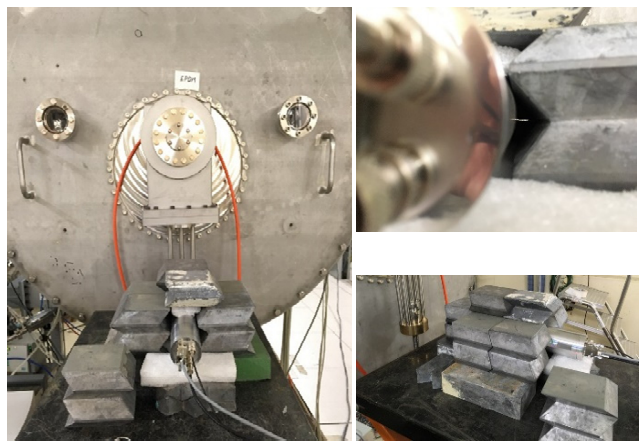

Figure 5: NaI(Tl) scintillator set up during cryomodule test, shielding and collimator aperture are shown respectively on the bottom-left and top-right corner of the figure.

DATA ANALYSIS AND SIMULATION

In this section two case studies will be presented: one concerning a high beta vertical test and another concerning a medium beta test in the MECCTD. The analysis is performed by means of particle tracking code [8], electrons are followed from the emitter (typically on the cavity iris) to the landing point. A set of 50 emitters, 1 mm distant from one another, are placed on each iris. The RF phase is scanned with 1° step.

The electron energy at the impact, their impact angle and position are recorded along with the RF phase and the departure point. The data are then post-processed by a set of Gnuplot scripts.

Vertical test

Figure 6 presents the results obtained from the cavity test in the vertical cryostat. It can be noted that despite the high radiation dose rate, the cavity quality factor starts to have a sensible slope above 18 MV/m, while field emission already started around 11 MV/m.

The data collected by the scintillator while the cavity was kept at 13 MV/m in the π-mode is shown in Fig. 7. This value was chosen in order to reduce the detector pile-up and dead time. It can been seen that the end point energy

ISBN: 978-3-95450-211-0 doi:10.18429/JACoW-SRF2019-THP097

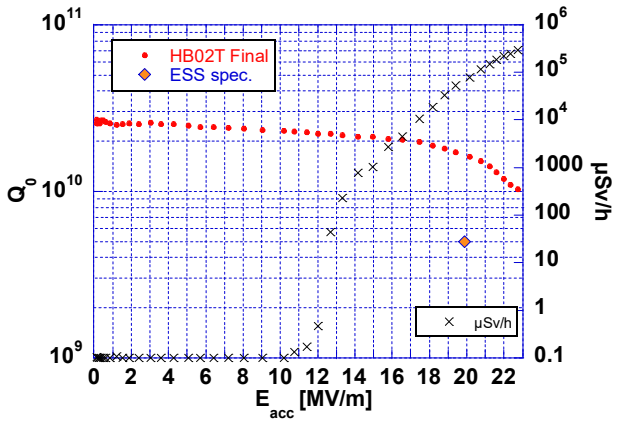

Figure 6: HB02T Q0 with respect to the accelerating field along with radiation dose measurements performed with G-M detector.

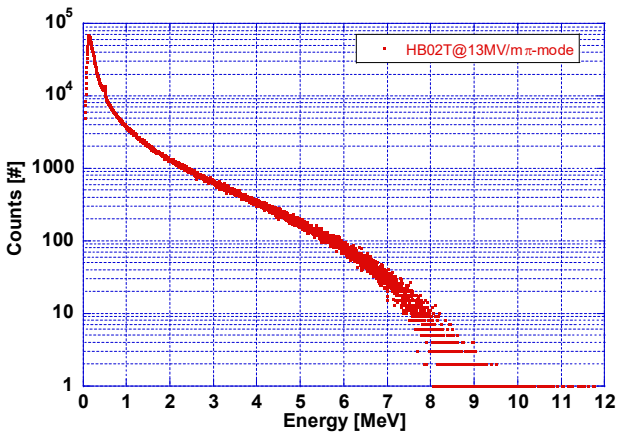

Figure 7: Data collected with the scintillator detector during the cavity power rise, the electric field was kept at 13 MV/m in the π-mode.

of the bremsstrahlung spectrum is approximately between 8 and 9 MeV.

The data collected by the PIN diodes are shown in Fig. 8. These were recorded when the detected dose rate was about 24 mSv/h and electric field in the cavity about 19 MV/m.

The red columns represent the signal from the PIN diodes on the cavity top flange while the black columns are the signal from the bottom flange. It should be pointed out that a peak appears on the meridian corresponding to the PIN number 5 (both top and bottom), this PIN is located on the main coupler port meridian.

All these collected information by the different detectors are then used as input to evaluate the simulation results. Figure 9 shows the impact location for a set of emitters located on the 4th iris, Z axis represent electron energy impact and colours are proportion to the amount of current of each trajectory (green corresponds to low current and red to high).

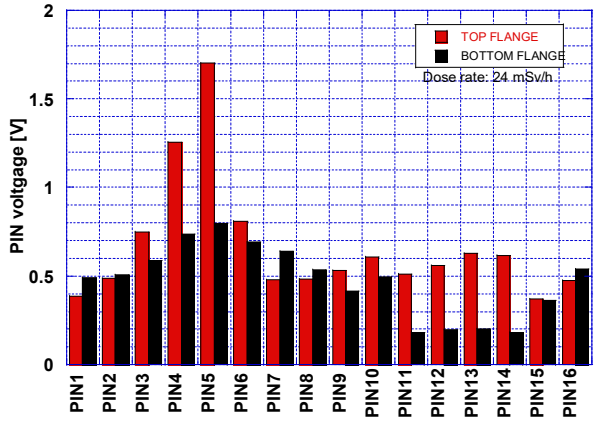

Figure 8: PIN diodes measurements during HB02T vertical test, top flange diodes (red columns) and bottom flange diodes (black columns), dose rate was about 24 mSv/h.

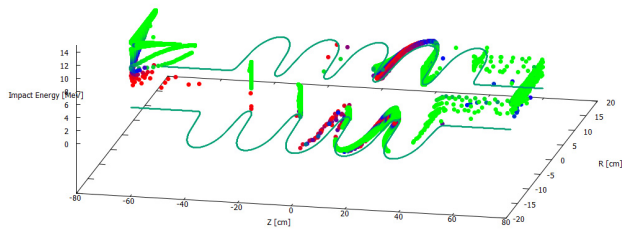

Figure 9: High beta cavity particle tracking, emitters are located on the 4th iris (from left), E_{acc}=13MV/m, trajectories are calculated at each 1° phase step. X-Y axis are used for cavity geometry and impact location, Z axis is used for impact energy and colours from green to red are used in proportion with the electron current computed by Eq. (1) (green=low current, red=high current).

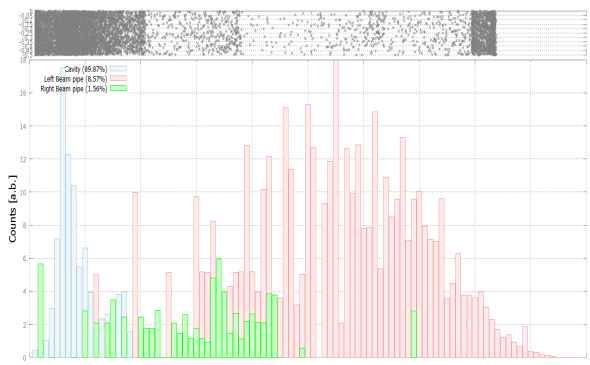

Figure 10: Energy spectra from particle tracking on high beta cavity with emitters located on 4th iris and accelerating field of 13 MV/m, red and green bins represent trajectories that end on the cavity beam pipes while blue bins represent impact location inside the cavity. Binning is done every 100 keV and the counting is proportional to Eq. (1).

The particle tracking simulation (Fig. 10) showed that emitters located on the 4th iris can emit electrons to both beampipe flanges (top and bottom). Approximately 90% of the emitted electrons remain inside the cavity and impact the surface with energy around 1-2 MeV. Only 10% of the

ISBN: 978-3-95450-211-0 doi:10.18429/JACoW-SRF2019-THP097

emitted electrons escape (8.5% from one side and 1.5% from the other) with impact energy up to 9 MeV.

The comparison of the test data and simulation allows an estimation of the location of the emitters. This latter is around the 4th iris on the main coupler meridian. To obtain a more precise location, it will be necessary to improve our detection capability, especially to capture the radiation produced by the impact of the electrons trapped inside the cavity.

Cryomodule

In this section, the data from a medium beta cavity (CAV3) tested in the cryomodule prototype (MECCTD) will be discussed. In Fig. 11 is shown the cavity accelerating field (purple line) along with the radiation dose rate (brown line). The cavity accelerating field was maintained at 16.7 MV/m with the nominal RF pulse length (3.6 ms) and repetition rate (14 Hz), during this phase the radiation dose oscillate between 2 mSv/h and 3 mSv/h.

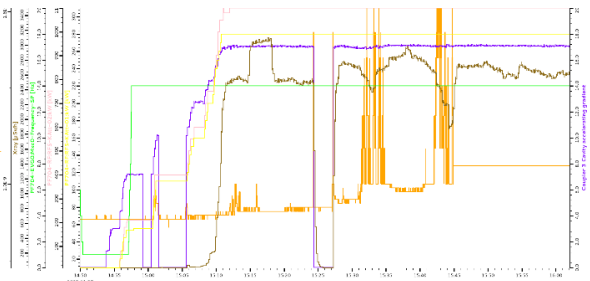

Figure 11: CAV3 during MECCTD, accelerating field (purple), radiation dose rate (brown) with respect to time.

The radiation dose rate detected for each cavity at 16.7 MV/m with the nominal RF pulse is given in Table 2. Each cavity has a radiation dose of some mSv/h, which is higher to the same measure performed during the test in the vertical cryostat. The origin of this deterioration is under investigation.

Table 2: Radiation Dose Rate at Nominal RF Pulse and Accelerating Field

Cavity number	Dose rate [mSv/h]
CAV 1	~7
CAV 2	~5
CAV 3	2-3
CAV 4	~3

The data collected with the scintillator positioned at one end of the cryomodule (see Figs. 4 and 5) are shown on Fig. 12. The end point energy of the bremsstrahlung spectrum is about 6 MeV.

The same procedure as the one used in the previous section was implemented to interpret the cryomodule test data.

The impact locations are shown in Fig. 13. They correspond to emitters located on the 2nd and 4th iris (from left) in a medium beta cavity.

Both emitter locations appear compatible with the bremsstrahlung detected with the scintillator. Figure 14 presents the energy spectra computed from both locations. Electrons coming from the 2nd iris have a maximum energy of about 6 MeV, with a peak about 5 MeV, while the electrons coming from the 4th iris have a maximum energy about 7.5 MeV with a peak around 6.5 MeV.

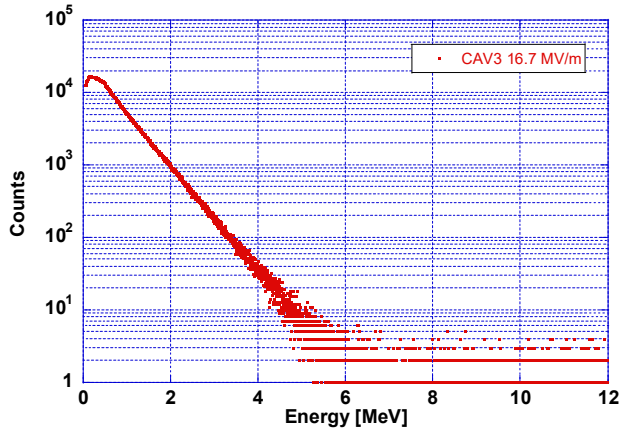

Figure 12: Data collected with the scintillator detector during the CAV3 operation, the electric field was kept at 16.7 MV/m with an RF pulse of 3.6 ms length and 14 Hz repetition rate.

SUMMARY AND OUTLOOK

CEA Saclay is continuously improving the detection capability for both vertical and cryomodule test stand. X-ray data collected during cavity vertical cryostat and cryomodule test were presented and analysed by means of particle tracking simulation. A systematic analysis was carried out allowing to identify the most probable location for the origin of the field emission.

In the future, more detectors will be added to gain a more detailed view of the radiation distribution around the cavities and hence a more precise location of field emission sources.

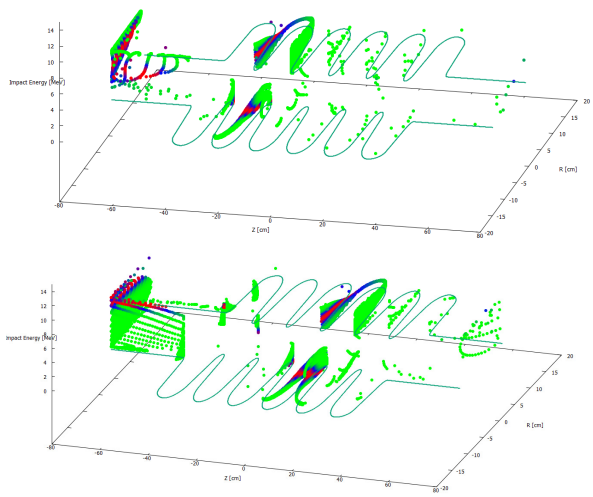

Figure 13: Medium beta cavity particle tracking, emitters are located on the 2nd iris (top) and 4th iris (bottom), Eacc=17MV/m, trajectories are calculated at each 1° phase step. X-Y axis are used for cavity geometry and impact location, Z axis is used for impact energy and colours from green to red are used in proportion with the electron current computed by Eq. (1).

ISBN: 978-3-95450-211-0 doi:10.18429/JACoW-SRF2019-THP097

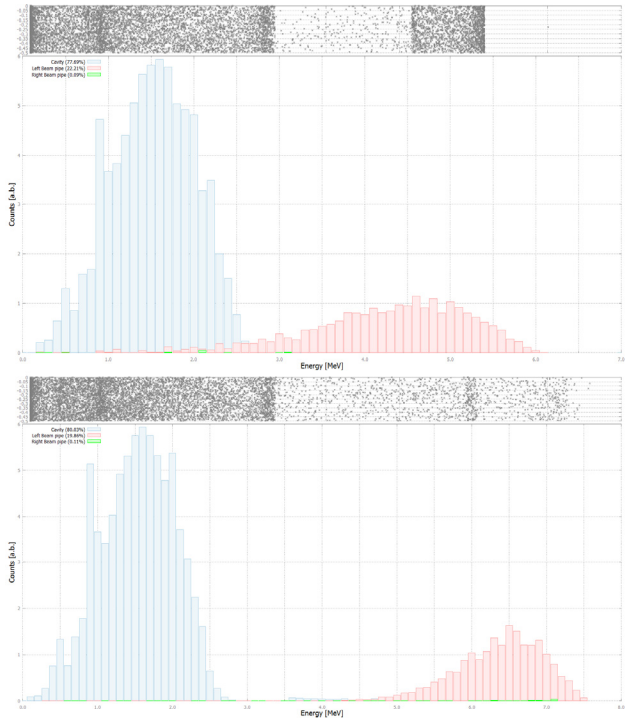

Figure 14: Histogram for impact energy computed for electron trajectories generated from the 2nd iris (top) and 4th iris (bottom). Binning is done every 100 keV the counting is proportional to Eq. (1), red and green bins represent trajectories that end on the cavity beam pipes while blue bins represent impact location inside the cavity.

REFERENCES

[1] E. Cenni *et al.*, "ESS Medium Beta Cavity Prototypes Manufacturing", in *Proc. SRF'15*, Whistler, Canada, Sep. 2015, paper THPB028, pp. 1136-1140.

[2] J. Plouin and G. Devanz, "Conceptual Design of the β = 0.86 Cavities for the Superconducting Linac of ESS", in *Proc. SRF'11*, Chicago, IL, USA, Jul. 2011, paper MOPO041, pp. 180-183.

[3] G. Devanz *et al.*, "ESS Elliptical Cavities and Cryomodules", in *Proc. SRF'13*, Paris, France, Sep. 2013, paper FRIOC02, pp. 1218-1222.

[4] R. H. Fowler and L. Nordheim, "Electron emission in intense electric fields," in *Proc. R. Soc. Lond. Ser. Contain. Pap. Math. Phys. Character*, vol. 119, no. 781, pp. 173–181, May 1928.

[5] H. Sakai et al., "Field Emission Studies in Vertical Test and During Cryomodule Operation using Precise X-ray Mapping System," Phys. Rev. Accel. Beams, vol. 22, no. 2, p. 022002, Feb. 2019.

[6] E. Cenni *et al.*, "Field Emission Simulation for KEK-ERL 9-Cell Superconducting Cavity", in *Proc. IPAC'12*, New Orleans, LA, USA, May 2012, paper MOPPC070, pp. 295-297.

[7] E. Cenni *et al.*, "Field Emission Measure During cERL Main Linac Cryomodule High Power Test in KEK", in *Proc. SRF'13*, Paris, France, Sep. 2013, paper TUP091, pp. 678-682.

[8] G. Wu, https://code.google.com/archive/p/fishpact/